Zero-Energy Photoelectric Effect

Sajad Azizi, Ulf Saalmann, and Jan M. Rost

Max-Planck-Institut für Physik komplexer Systeme, Nöthnitzer Straße 38, 01187 Dresden, Germany

We predict a near-threshold ("zero energy") peak in multiphoton ionization for a dynamical regime where the photon frequency is large compared to the binding energy of the electron. The peak position does not depend on the laser frequency but on the binding energy and the pulse duration. The effect originates from the fact that bound-continuum dipole transitions are stronger than continuum-continuum ones. To clearly observe this zero-energy photoelectric effect, the spectral width of the laser pulse should be comparable to the binding energy of the ionized orbital, and the second ionization potential should be larger than the photon energy. This suggests negative ions as ideal candidates for corresponding experiments.

A threshold for an observable A indicates the transition of the system from one regime to another upon change of the relevant parameter ε and therefore provides important information about the system. Often, the observable changes near threshold at ε_0 with a certain power of the parameter, i.e., $A(\varepsilon \to +\varepsilon_0) \propto (\varepsilon/\varepsilon_0 - 1)^\alpha$. Probably best known are thermodynamical variables near phase transitions [1], but quantum critical points in condensed matter [2] or fragmentation and ionization thresholds in atomic and molecular physics [3] are also examples. In the latter case the so-called Wigner threshold law [4] for fragmentation cross sections of particles under short-range forces is a universal property, similar to its counterpart for long-range (Coulomb) forces, the Wannier law [5,6].

The Wigner law has been verified in fragmentation scenarios including multiphoton detachment of a negative ions [7], which were a popular target for theoretical considerations [8] regarding above-threshold ionization (ATI). However, so far it has gone unnoticed that the combination of the Wigner threshold behavior with *short* intense pulses can give rise to a peculiar zero-energy photoelectric effect (ZEPE) with a characteristic maximum, whose position at very low photo-electron energy does not depend on the photon energy but on the duration of the (short) laser pulse. That short intense pulses can lead to unusual electron dynamics has been pointed out in the context of nonadiabatic photoionization [9,10] where short pulses can even be used for coherent control [11].

The ZEPE effect requires pulses short enough such that their spectral bandwidth ΔE is larger than the binding energy E_{EA} of the detached electron, typically of the order of a few femtoseconds. This was clearly not the case in the ATI detachment experiments with 800 nm light. ZEPE is enabled by a two-photon process, where a bound electron absorbs a photon and emits a photon, ending at the same (bound) energy as it started from. Therefore, this mechanism does not typically contribute to the photo-electron spectrum. However, if the laser pulse is short enough that the spectral peak at the binding energy "leaks" into the continuum (see Fig. 1), this process becomes visible in form of photo electrons and can lead, together with the Wigner power law, to a pronounced ZEPE maximum.
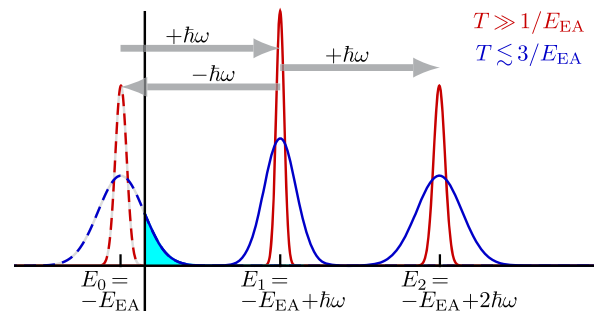
FIG. 1. Multiphoton detachment of a an electron, weakly bound by electron affinity E_{EA} to an ion, will give rise to peaks in the photo-electron spectrum at energies $E = -E_{\mathrm{EA}} + n\omega$, shown here for $n = 1, 2$. However, following absorption of the first photon it is more likely that a second photon is not absorbed but emitted ($-\hbar\omega$) since the bound-continuum $|E_0\rangle \to |E_1\rangle$ transition dipole is much stronger than the continuum-continuum $|E_1\rangle \to |E_2\rangle$ transition dipole. This process with net-zero energy absorption only becomes visible in the spectrum for very short pulses (blue) leading to a broad peak at $-E_{\mathrm{EA}}$, whose tail reaches into the continuum (light blue shaded) but not for longer pulses (red).

Negative ions are an ideal target to clearly identify the ZEPE, since they combine a low electron affinity (EA), i.e., the ionization potential of the negative ion, with a typically large gap to the next ionization potential (IP), i.e., the ionization potential of the (neutral) atom. Therefore, a relatively large photon frequency, still fulfilling $E_{EA} < \omega < E_{IP}$, can be chosen, which on the one hand prevents ionization of more deeply bound electrons and on the other hand lets the first ATI peak appear at relatively high energy, keeping an energy interval just above threshold pristine for a clean signature of ZEPE.

We will demonstrate the effect in the following with negative ions of hydrogen and oxygen in a simple and transparent fashion. To this end, we use an effective potential for the bound electron of the negative ion which is designed to reproduce the EA well [12,13],

$$V(r) = -\frac{Z}{r}\frac{b}{1 + c[\exp(r/r_0) - 1]}, \quad (1)$$

where Z is the nuclear charge. It is $Z = 1$ and $Z = 8$ for hydrogen and oxygen, respectively. We use atomic units unless stated otherwise. With parameter values $b = 1.1$, $c = 1$, and $r_0 = 0.5292$ Å the computed $E_{1s} = -0.75$ eV for H$^-$ closely matches the experimental value [14]. Similarly, with $b = 1$, $c = 1.9607$, and $r_0 = 0.4689$ Å, the computed $E_{2p} = -1.464$ eV for O$^-$ is in good agreement with the experimental value of -1.461 eV [15].

With the potential (1) the Hamilton operator reads

$$\hat{H}(t) = \hat{p}^2/2 + V(r) + \hat{p} \cdot e_z A_0 g(t) \cos(\omega t), \quad (2)$$

where $g(t) = \exp(-t^2/T^2)$ is the laser-pulse envelope with the pulse duration $T = T_{fwhm}/\sqrt{2\ln 2}$, linearly polarized along the z axis and dipole coupled in velocity gauge. In single-active-electron approximation (2), the propagation of the 3D time-dependent Schrödinger equation (TDSE), for processes discussed here, is straightforward, since the number of photons involved is moderate. What is challenging, however, is the numerically accurate description of the *very* small detachment probabilities close to threshold. To this end we calculate eigenstates and dipole matrix elements for the potentials given in (1) for $\ell = 0 \ldots \ell_{max}$ in a box $r = 0 \ldots R$ up to a cutoff energy E_{cut}. The parameters used are $\ell_{max} = 4$, $R = 3 \times 10^3$ Å and $E_{cut} = 3$ keV. The TDSE is propagated numerically with this field-free basis. From the final amplitudes obtained we calculate the photoelectron spectrum. Attaching to every eigenstate a normalized Gaussian, whose height is the absolute square of the amplitude and whose width is given by the level spacing at the corresponding eigenenergy, produces a continuous spectrum. Thereby, the density of states and the detachment process are correctly included.
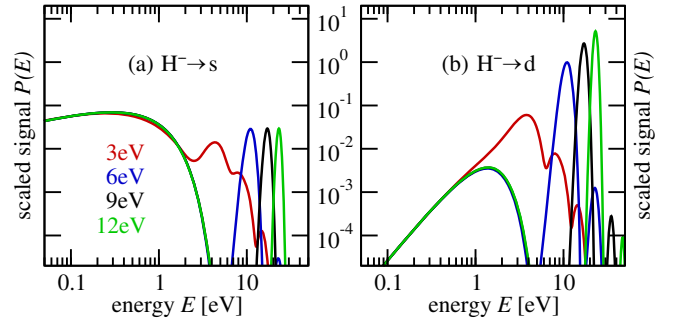
FIG. 2. Spectra from H$^-$ for $T_{fwhm} = 1$ fs, $I = 10^{14}$ W/cm^2 and 4 different photon frequencies ($\omega = 3, 6, 9, 12$ eV). We show electrons in the s-continuum (a) and the d-continuum (b), respectively. Note, while higher-order peaks (at energies $E \gtrsim 6$ eV) shift with increasing ω to higher energies, the zero-peak position ($E_s \approx 0.3$ eV and $E_d \approx 1.4$ eV) is independent of ω. Spectra are scaled such that they agree for $E = 0.1$ eV.

Figure 2 shows the resulting photo-electron spectra for H$^-$ exposed to a laser pulse of 1 fs duration and a peak intensity of $I = 10^{14}$ W/cm^2 for different photon frequencies. The unique feature of the zero-energy photoeffect is evident: There is a pronounced maximum close to threshold ($E_s \approx 0.3$ eV and $E_d \approx 1.4$ eV) which is independent of the photon frequency, clearly different in shape from the two-photon ATI peaks which can be identified at the respective energies $E = 2\omega - E_{EA}$. If the ZEPE maximum is much smaller than and too close to the ATI peaks, typically for higher final partial waves $\ell > 0$, then it may get buried under the rise to the two-photon ATI peak, which is the case for H$^-$ → d detachment with 3 eV photons, as visible in Fig. 2(b).

To understand how ZEPE comes about qualitatively and quantitatively, we take a closer look at the near-threshold energy range with the spectra of Fig. 3 on a linear scale for different pulse durations T. One immediately sees that the spectra depend on T, as already anticipated. The Wigner threshold law [4] states that for breakup of two fragments under short-range forces (which is the case for electron detachment), the ionization probability near threshold does *not* depend on the respective process but has a universal shape given by the available continuum states in momentum space, i.e.,

$$P(E \to 0) \propto \int dp \, p^{2(\ell+1)} \delta(p^2/2 - E) \propto E^{\ell+1/2}, \quad (3)$$

where ℓ is the angular momentum of the fragment pair. Following the intuition that ZEPE originates in the combination of the Wigner law and a Gaussian energy distribution induced by the short laser pulse, located at the binding energy $-E_{EA}$ due to the two-photon zero-energy process, the detachment probability should be given by (see also Appendix A)
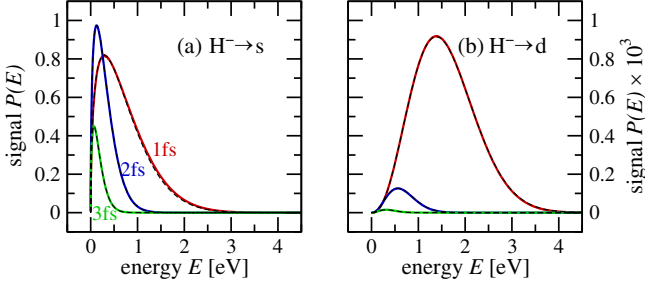
FIG. 3. Photo-electron spectrum (colored solid lines) of H$^-$ for a Gaussian pulse with different pulse duration $T_{\text{fwhm}} = 1, 2, 3$ fs, carrier frequency $\omega = 9$ eV, and intensity $I = 10^{14}$ W/cm^2 for the s (a) and the d-channel (b), respectively, and fits (black dashed lines) according to Eq. (4).

$$P_{\text{ZEPE}}^{\ell,\beta}(E) = P_*(E)s_{\ell,\beta}(E/E_{\text{EA}}), \qquad (4)$$

$$P_*(E) = [1 + E/E_*]^{-1} \qquad (4a)$$

$$s_{\ell,\beta}(x) = \beta^4 x^{\ell+\frac{1}{2}} \exp(-\beta^2[x+1]^2). \qquad (4b)$$

The universal shape $s_{\ell,\beta}(x)$ of the zero-energy photo-electron spectrum is fully determined by the angular momentum ℓ of the photo electron and $\beta = E_{\text{EA}}/\Delta E$ the ratio of electron affinity E_{EA} to spectral pulse width ΔE. From the spectral representation of the pulse and the fact that ZEPE is a two-photon process $\Delta E = 2/T$ follows, which is confirmed by second-order perturbation theory discussed below. Furthermore, $P_*(E)$ takes care of the slowly varying background, being different for each ion.

The dashed lines in Fig. 3 show $P_{\text{ZEPE}}^{\ell,\beta}(E)$ according to Eq. (4). The only fit parameter E_* assumes the values $E_* = 0.896$ eV and $E_* = 0.684$ eV for the "s" and "p" photo electrons of hydrogen and oxygen, respectively, while $E_* = 13.4$ eV and $E_* > 1000$ eV for the electrons detached with angular momentum "d" and "f" reveal that the background is nearly constant in these cases over the energy interval considered. Obviously, Eq. (4) represents

the numerical results very well, giving confidence in the interpretation and description of ZEPE provided. Deviations for O$^-$ at "longer" pulses can be attributed to higher-order effects occurring for intense pulses, since the agreement with the analytic description for a weaker pulse with $I = 10^{12}$ W/cm^2, as shown by the gray line in Fig. 4(c), is excellent.

Peculiar at second glance is the variation of the maximal detachment with the pulse length T or ΔE, respectively. Note that the highest maximum is achieved in Fig. 3 with $T_{\text{fwhm}} = 2$ fs for the $\ell = 0$ case, while for all other ℓ the maxima seem to increase monotonically. To elucidate their behavior systematically (see also Appendix B), we determine the maximum of $P_{\text{ZEPE}}^{\ell,\beta}$ with respect to the two-dimensional parameter space $\{\beta, x\}$, i.e., the (scaled) pulse width $\beta = E_{\text{EA}}/\Delta E$ and the (scaled) excess energy $x = E/E_{\text{EA}}$. The corresponding optimal parameters, obtained from vanishing derivatives with respect to β and x, are given by analytical but lengthy expressions. Inserting $\beta(x) = \sqrt{2}/(1+x)$, the solution of the first condition $\partial P_{\text{ZEPE}}^{\ell,\beta}/\partial\beta = 0$, into the second condition $\partial P_{\text{ZEPE}}^{\ell,\beta}/\partial x = 0$ gives an analytical but lengthy expression for $\beta_{\text{Max}}(x^*,\ell)$, i.e. the pulse width that gives the highest peak of the detachment probability.

Ignoring the background modification (4a) by taking the limit $x^* \to \infty$ one obtains with the simpler expressions $\beta_{\text{Max}} = (7 - 2\ell)/4\sqrt{2}$ and $x_{\text{Max}} = (1 + 2\ell)/(7 - 2\ell)$ directly the optimal pulse duration $T_{\text{fwhm}} = \sqrt{8\log 2}\beta_{\text{Max}}/E_{\text{EA}}$. The values are 2.55 fs and 1.09 fs for H$^-$ (s and d channel) and 0.92 fs and 0.18 fs for O$^-$ (p and f channel), consistent with the data shown in Fig. 4. Within the same approximation one can determine the location of the maxima of $P_{\text{ZEPE}}^{\ell,\beta}$ for a given pulse durations β. They read

$$E_{\text{max}} = \frac{E_{\text{EA}}}{2}\left(\sqrt{1 + (2\ell + 1)/\beta^2} - 1\right) \qquad (5)$$
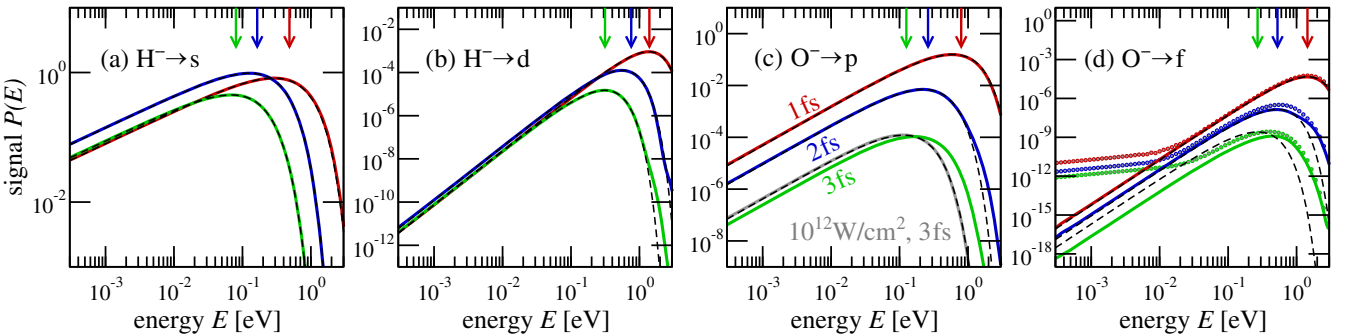
FIG. 4. Photo-electron spectra for H$^-$ (a),(b) as in Fig. 3 but also for the two final channels of O$^-$ (c),(d) in double-logarithmic scale. Note the different vertical scale for each panel. The gray line in panel (c) is for a lower intensity of $I = 10^{12}$ W/cm^2 and therefore scaled by a factor of 10^4. The dotted lines in panel (d) are computed with a basis of states up to $E_{\text{cut}} = 30$ eV which would allow to describe three-photon processes; the solid curves are for $E_{\text{cut}} = 3$ keV. Arrows mark the maxima according to Eq. (5).

TABLE I. Total ionization probability P_T for H$^-$ and O$^-$ for accessible channels and three pulse durations T_{fwhm}.

	H$^-\to$ s	H$^-\to$ d	O$^-\to$ s	O$^-\to$ d
$T_{\text{fwhm}} = 1$ fs	8.9×10^{-4}	1.5×10^{-6}	1.8×10^{-4}	7.1×10^{-8}
2 fs	4.4×10^{-4}	9.1×10^{-8}	3.1×10^{-6}	9.7×10^{-11}
3 fs	1.1×10^{-4}	6.4×10^{-9}	3.9×10^{-8}	6.8×10^{-13}

FIG. 5. Photo-electron spectra in linear (a) and double-logarithmic (b) scale for the f channel of O$^-$ from TDSE calculations (ω and I as in Fig. 3, $T_{\text{fwhm}} = 1$ fs) with different cutoff energies E_{cut} (see text).

and are shown in Fig. 4 for the respective pulses with vertical arrows. Although for $\ell = 0$ (H$^-$) and $\ell = 1$ (O$^-$) the background is relevant, since E_* is in the energy range of interest, the values (5) explain the maxima there quite well.

Hence, the overview of ZEPE for H$^-$ and O$^-$ in Fig. 4, highlighting the influence of different partial waves $\ell = 0, \ldots, 3$ of the fragments, reveal that essentially all features discussed so far can be identified and are confirmed. For completeness we estimate the number of ZEPE electrons per shot one could detect in an experiment,

$$N_{\text{exp}} = N_{\text{ion}}[I_{\text{exp}}/10^{14}\ \text{W/cm}^2]^2 P_T, \qquad (6)$$

where N_{ion} is the number of ions in the target volume, I_{exp} the experimental laser intensity, and P_T is given in Table I.

The double-logarithmic scale in Fig. 4 was chosen to emphasize the threshold behavior, and one can see that the quasianalytical formula (4) performs in all cases extremely well compared to the numerical TDSE calculations, particularly with regard to the large dynamic ranges

considered. In fact, the TDSE results in Fig. 4(d) contain a surprise: they appear not to be converged for the $\ell = 3$ spectrum of oxygen. Indeed, despite very small photo electron energies of the order of 1 meV, numerically one has to include continuum electrons up to 3 keV to achieve convergence (see also Fig. 5).

Since ZEPE is dominantly a two-photon process as corroborated by its dependence on laser intensity (see Appendix C), it should also be understandable with second-order perturbation theory comprising the two different events of absorption of a photon followed by emission ($\eta = $ " $+$ ") of a photon, typically much stronger than emission followed by absorption ($\eta = $ " $-$ "). The ionization amplitude to energy E for these processes reads [16]

$$
\begin{aligned}
a(E) &= \sum_k d_{Ek} d_{k\,\text{EA}} \int_{-\infty}^{+\infty} dt A(t) e^{i[E-E_k]t} \int_{-\infty}^{t} dt' A(t') e^{i[E_k+E_{\text{EA}}]t'} \\
&= \frac{\pi}{8} T^2 A_0{}^2 \sum_k d_{Ek} d_{k\,\text{EA}} \sum_{\eta=\pm} \left[e^{-[[\Delta_k^\eta + E_{\text{EA}}]^2 + [E - \Delta_k^\eta]^2]T^2/4} - \frac{2i}{\sqrt{\pi}} e^{-[E+E_{\text{EA}}]^2 T^2/8} F([2\Delta_k^\eta + E_{\text{EA}} - E]T/\sqrt{8}) \right]
\end{aligned} \qquad (7)
$$

with the dipole matrix elements $d_{jk} \equiv \boldsymbol{e}_z \cdot \langle \phi_j | \boldsymbol{d} | \phi_k \rangle$ and the detunings $\Delta_k^\pm \equiv E_k \mp \omega$. We have not explicitly specified that $|\phi_0\rangle$, $|\phi_k\rangle$, $|\phi_E\rangle$ have different angular momenta ℓ, dictated by selection rules in the dipole matrix elements, and for simplicity we have assumed that all virtual states $|\phi_k\rangle$ are discrete in accordance with our numerical treatment of the continuum. Finally, due to the necessary cutoff at E_{cut}, the sum over virtual states k is finite. From the real part of (7) one sees that continuum states, which are resonant with initial one-photon absorption $\Delta_k = 0$, are dominant as well as the final energy equal to the initial energy, $E = -E_{\text{EA}}$, as expected for the zero-energy photo-electric effect.

Coming back to the requirement of including very high energies E_k in the calculation to reach convergence for small finite energy E, we note that the Dawson function

F [17] in the imaginary part of Eq. (7) falls off very slowly $F(x) \sim 1/(2x)$ for large x. That implies that nonresonant states $E_k \gg E$ can contribute significantly. Since the detachment probability $\propto (E/E_{\text{EA}})^{\ell+1/2}$ is very small near threshold, it must be determined with high absolute accuracy, which explains why unexpectedly high virtual energies need to be taken into account. Note, that for the very same reason the two-photon process of first *emitting* and then absorbing a photon, in standard situations never considered, has a non-negligible contribution.

In summary, we have discussed a universal two-photon process optimally observable in negative ions, where the weakly bound electron after absorption and emission of one photon returns to approximately its initial energy. If a short (broadband) pulse is employed, part of the spectrum will leak into the continuum. Together with the typical Wigner

power law of the electron-detachment cross near threshold, a characteristic maximum forms at very low electron energies, which does not dependent on the photon frequency, as accurate numerical calculations confirm. They require the inclusion of surprisingly energetic electronic continuum states to converge, highlighting subtle features of this unconventional process which also surface in second-order time-dependent perturbation theory. Following physical intuition, we have derived an analytical form of the spectrum. It describes the relative peak height and location as well as the dependence on pulse length and electron affinity of this peculiar zero-energy photoelectric effect very well, which will facilitate its experimental realization.

---

[1] H. E. Stanley, *Introduction to Phase Transitions and Critical Phenomena*, International Series of Monographs on Physics (Oxford University Press, New York, 1971).

[2] S. Sachdev, *Quantum Phase Transitions* (Cambridge University Press, Cambridge, England, 2000).

[3] J. M. Rost, Critical phenomena in atomic physics, Physica (Amsterdam) **9E**, 467 (2001).

[4] E. P. Wigner, On the behavior of cross sections near thresholds, Phys. Rev. **73**, 1002 (1948).

[5] G. H. Wannier, The threshold law for single ionization of atoms or ions by electrons, Phys. Rev. **90**, 817 (1953).

[6] J. M. Rost, Two-electron escape near threshold: A classical process?, Phys. Rev. Lett. **72**, 1998 (1994).

[7] R. Reichle, H. Helm, and I Yu. Kiyan, Photodetachment of H^- in a strong infrared laser field, Phys. Rev. Lett. **87**, 243001 (2001).

[8] K. Krajewska, I. I. Fabrikant, and A. F. Starace, Threshold effects in strong-field detachment of H^- and F^-: Plateau

[9] K. Toyota, O. I. Tolstikhin, T. Morishita, and S. Watanabe, Slow electrons generated by intense high-frequency laser pulses, Phys. Rev. Lett. **103**, 153003 (2009).

[10] Q.-C. Ning, U. Saalmann, and J. M. Rost, Electron dynamics driven by light-pulse derivatives, Phys. Rev. Lett. **120**, 033203 (2018).

[11] S. Azizi, U. Saalmann, and Jan M. Rost, Non-adiabatic ionization with tailored laser pulses, J. Phys. B **54**, 134001 (2021).

[12] P. S. Ganas, J. D. Talman, and A. E. S. Green, Independent-particle models for light negative atomic ions, Phys. Rev. A **22**, 336 (1980).

[13] R. Shakeshaft and X. Tang, Integral-equation approach to multiphoton ionization by intense fields. II. Application to H and H^-, Phys. Rev. A **36**, 3193 (1987).

[14] K. R. Lykke, K. K. Murray, and W. C. Lineberger, Threshold photodetachment of H^-, Phys. Rev. A **43**, 6104 (1991).

[15] M. K. Kristiansson *et al.*, High-precision electron affinity of oxygen, Nat. Commun. **13**, 5906 (2022).

[16] S. Azizi, Three aspects of photo-ionization in ultrashort pulses, Ph.D. thesis, Technische Universität Dresden, 2023.

[17] The Dawson function $F(z)$ [18] is related to the (complex) error function, $F(z) = (\sqrt{\pi}/2i)e^{-z^2} \mathrm{erf}(iz)$.

[18] H. G. Dawson, On the numerical value of $\int_0^\infty dx\, e^{x^2}$, Proc. London Math. Soc. **XXIX**, 519 (1897).

[19] J. M. Rost and T. Pattard, Analytical parametrization for the shape of atomic ionization cross sections, Phys. Rev. A **55**, R5 (1997).

[20] J. M. Rost and T. Pattard, Universal shape function for the double-ionization cross section of negative ions by electron impact, J. Phys. B **32**, L457 (1999).

[21] T. Pattard, A shape function for single-photon multiple ionization cross sections, J. Phys. B **35**, L207 (2002).

End Matter

APPENDIX A

The considerations leading to Eqs. (4) are the following. We know the behavior of the ZEPE spectrum for small and large excess energies E analytically. (i) According to the Wigner threshold law, see Eq. (3), the detachment probability must vanish for $E \to 0$ as $P(E) \sim E^{\ell+1/2}$. (ii) In the opposite limit of large energies $E \gg 1/T$ the detachment probability is suppressed by the finite spectral width of the laser pulse $P(E) \sim T^4 e^{-[E+E_{\mathrm{EA}}]^2 T^2/4}$, as has been quantified in Eq. (7). Therefore, the product of these two functions describes the dominant dependence on excess energy E. (iii) However, such kind of dynamics typically sits on a background which slowly decreases with increasing E. We parameterize this cross section with $P_*(E)$, where E_* controls the decrease of $P_*(E)$. We have formulated similar shape functions successfully in the past for electron impact ionization and photo double ionization near threshold with

three charged fragments in the final channel [19–21], where the threshold behavior is governed by the Wannier threshold law [5,6]. By combining (i–iii) and introducing dimensionless quantities $\beta = E_{\mathrm{EA}}/\Delta E$ with $\Delta E = 2/T$ we arrive at Eqs. (4).

APPENDIX B

Since $P_*(E)$ is slowly varying, we can determine the position of the maxima and their dependence on the pulse duration analytically to a good approximation by neglecting the dependence on $P_*(E)$, using the expression

$$\tilde{P}_{\mathrm{ZEPE}}^{\ell,\beta}(E) = \beta^4 x^{\ell+\frac{1}{2}} \exp(-\beta^2[x+1]^2)|_{x=E/E_{\mathrm{EA}}}. \quad (B1)$$

The maxima are obtained from the vanishing derivative with respect to $x (= E/E_{\mathrm{EA}})$. The highest maximum occurs when the derivative with respect to $\beta(= E_{\mathrm{EA}}/\Delta E)$ vanishes

as well. By looking first at the latter one obtains

$$\frac{\partial}{\partial\beta}\tilde{P}^{\ell,\beta}_{\text{ZEPE}} = [4/\beta - 2\beta[x+1]^2]\tilde{P}^{\ell,\beta}_{\text{ZEPE}} = 0, \qquad \text{(B2a)}$$

i.e., $\beta = \sqrt{2}/[1+x]$ as stated in the text. Note that this relation even holds for the more general $P^{\ell,\beta}_{\text{ZEPE}}$.

Similarly, it is

$$\frac{\partial}{\partial x}\tilde{P}^{\ell,\beta}_{\text{ZEPE}} = [[\ell+1/2]/x - 2\beta^2[x+1]]\tilde{P}^{\ell,\beta}_{\text{ZEPE}} = 0. \quad \text{(B2b)}$$

By combing the two conditions from Eqs. (B2) we arrive at the $\beta_{\text{Max}} = (7-2\ell)/4\sqrt{2}$ and $x_{\text{Max}} = (1+2\ell)/(7-2\ell)$, as stated in the text.

APPENDIX C

In order to show that the process considered is indeed of 2nd order, we show in Fig. 6 for H$^-$ the dependence of the
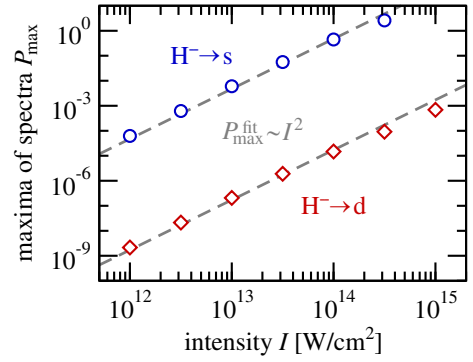
FIG. 6. Maxima P_{max} of the photo-electron spectra $P(E)$ for H$^-$ into the s (blue circles) and the d (red diamonds) channel as a function of the laser intensity I along with fits $P_{\text{max}}(I) \sim I^2$ (gray-dashed lines). The pulse duration is $T_{\text{fwhm}} = 3$ fs, the carrier frequency $\omega = 9$ eV.

maxima P_{max} in the spectra on the laser intensity I, which evidently scales with I^2.